Effects of stellar density on the photoevaporation of circumstellar discs

Concha-Ramírez, F.A.; Wilhelm, M.J.C.; Portegies Zwart, S.F.; Terwisga, S.E. van; Hacar, A.

MNRAS **000**, 1–14 (2020) Preprint 22 November 2021 Compiled using MNRAS LATEX style file v3.0

Effects of stellar density on the photoevaporation of circumstellar discs

Francisca Concha-Ramírez,[1]⋆ Martijn J. C. Wilhelm,[1] Simon Portegies Zwart,[1] Sierk E. van Terwisga,[2] Alvaro Hacar[1]
[1] *Leiden Observatory, Leiden University, PO Box 9513, 2300 RA Leiden, The Netherlands*
[2] *Max-Planck-Institut fÃijr Astronomie, KÃűnigstuhl 17, D-69117 Heidelberg, Germany*

Accepted XXX. Received YYY; in original form ZZZ

ABSTRACT
Circumstellar discs are the precursors of planetary systems and develop shortly after their host star has formed. In their early stages these discs are immersed in an environment rich in gas and neighbouring stars, which can be hostile for their survival. There are several environmental processes that can affect the evolution of circumstellar discs, and external photoevaporation is arguably one of the most important ones. Theoretical and observational evidence point to circumstellar discs losing mass quickly when in the vicinity of massive, bright stars. External photoevaporation can then constrain the time and material available to form planets. The stellar density of the region seems to influence the extent of the effects of external photoevaporation. In this work we perform simulations of star clusters with a range of stellar densities. Stars with masses $M_* \leq 1.9\ M_\odot$ are surrounded by a disc, and stars with masses $M_* > 1.9\ M_\odot$ are considered as emitting radiation. Our results show that external photoevaporation is efficient in depleting disc masses and that the degree of its effect is related to stellar density. Dense clusters have $\sim 10\%$ surviving discs by 2 Myr, whereas sparse ones have $\sim 50\%$. Surviving discs in sparser regions also span a larger range of masses. We compare our results to observations of the Lupus clouds, the Orion Nebula Cluster, the Orion Molecular Cloud-2, Taurus, and NGC 2024, and find that the trends observed between region density and disc masses are similar to those in our simulations.

Key words: protoplanetary discs – stars: planetary systems – stars: kinematics and dynamics – planets and satellites: formation – methods: numerical

1 INTRODUCTION

Circumstellar discs are the reservoirs of gas and dust that surround young stars and have the potential to become planetary systems. Their evolution will determine the time and material available to form planets. Studying the evolution of circumstellar discs can then help us understand planet formation and the diversity of observed planetary systems.

These circumstellar discs develop almost immediately after star formation, as a direct consequence of the collapse of a molecular cloud and angular momentum conservation (Williams & Cieza 2011). Their surroundings are rich in gas and neighbouring stars, which can be hostile to the discs and affect their evolution in different ways. In environments with high stellar densities, dynamical encounters with nearby stars can truncate the discs (e.g. Vincke et al. 2015; Portegies Zwart 2016; Bhandare & Pfalzner 2019). Face-on accretion of gas onto the circumstellar discs can cause them to shrink and increase their surface densities (e.g. Wijnen et al. 2016, 2017). Feedback from processes related to stellar evolution, such as stellar winds and supernovae explosions, can also truncate, tilt, or completely destroy the discs (Pelupessy & Portegies Zwart 2012; Close & Pittard 2017; Portegies Zwart et al. 2018). The presence of bright, massive stars in the vicinity of circumstellar discs can heat their surface enough to evaporate mass from them. This process, known as external photoevaporation, is arguably one of the most important environmental mechanisms in depleting mass in young circumstellar discs, and its effects seem to greatly outperform that of other means for disc truncation (e.g. Adams et al. 2004; Guarcello et al. 2016; Facchini et al. 2016; Haworth & Clarke 2019; Winter et al. 2019a; Haworth & Owen 2020).

The effects of external photoevaporation have been identified in observational surveys of young stellar objects in star-forming regions. Proplyds –cometary tail-like struc-

⋆ fconcha@strw.leidenuniv.nl

tures formed by ionized, evaporating discs– have been observed in particular in dense regions of the Orion nebula (O'dell & Wen 1994; O'dell 1998; Mann et al. 2014; Kim et al. 2016). Surveys of protoplanetary discs in star-forming regions suggest that discs closer to bright stars are less massive than their counterparts in sparser regions (Fang et al. 2012; Mann et al. 2014; Ansdell et al. 2017; van Terwisga et al. 2020), suggesting that discs in the vicinity of these stars are strongly affected by their environment. Disc fractions (the number of young stellar objects around which dust is detected, over the total number of objects) and disc mass distributions in younger and less dense star-forming regions, such as Lupus and Taurus, are statistically indistinguishable from each other in terms of disc mass distributions. The average disc mass in these regions is higher than in the Orion Nebula Cluster (Ansdell et al. 2016; Eisner et al. 2018; van Terwisga et al. 2019), which is a much denser environment.

In previous work (Concha-Ramírez et al. 2019, hereafter Paper I) we show that external photoevaporation is efficient in destroying circumstellar discs on a relatively short timescale. For regions of stellar densities $\sim 100 M_\odot pc^{-3}$, around 80% of discs have evaporated within 2.0 Myr of evolution. Between 25% and 60% of the discs, depending on region density, are destroyed within the first 0.1 Myr. We argue that the rapid decrease in disc mass is mostly caused by external photoevaporation, rather than dynamical truncations, and that the former mechanism constrains the time available for planet formation. Similar conclusions are drawn by Winter et al. (2019b) and Nicholson et al. (2019). The 'missing-mass problem', an observational discrepancy in which protoplanetary disc masses are lower than the masses of known rocky planetary systems, also suggests that planet formation is already ongoing in discs of ages as small as 1.0 – 3.0 Myr (Greaves & Rice 2010; Williams 2012; Najita & Kenyon 2014; Manara et al. 2018), or even earlier than 0.5 Myr (Tychoniec et al. 2020). Both the short lifetimes of circumstellar discs even in low radiation fields (Facchini et al. 2016) and the missing-mass problem point to planet formation starting shortly after circumstellar discs form.

Observational and theoretical evidence suggests that the stellar density of the surroundings is a key factor in the survival of circumstellar discs and in their eventual observed mass distributions. Understanding disc mass and size distributions in young star clusters is therefore paramount for understanding planet formation and evolution. Here we study the effects of external photoevaporation of circumstellar discs in star clusters, expanding the analyses of Paper I. We perform simulations of circumstellar discs embedded in star clusters of several different stellar densities, which are evolved for 2.0 Myr, and investigate the mass and size distributions of the eventual disc population before planet formation commences. We quantify the effect that stellar density has on the efficiency of external photoevaporation. We compare our simulation results to masses of dusty young stellar objects in the Lupus clouds (Ansdell et al. 2016, 2018), the Orion Nebula Cluster (Mann et al. 2014; Eisner et al. 2018), the Orion Molecular Cloud-2 (van Terwisga et al. 2019), the Taurus region (Andrews et al. 2013), and NGC 2024 (Getman et al. 2014).

2 MODEL

We use the Astrophysical Multipurpose Software Environment, AMUSE[1] (Portegies Zwart et al. 2009), to bring together codes for viscous disc evolution, stellar dynamics, and stellar evolution, along with an implementation of external photoevaporation. The setup and models used for the simulations in this paper is the same as in Paper I. In the present work we perform simulations spanning a larger range of stellar densities and increase the number of stars in each simulation. Below we present a summary of the simulation model; for details, the reader should refer to Paper I. All the code developed for the simulations, data analyses, and figures of this paper is available online[2].

2.1 Stars and circumstellar discs

We separate the stars in the simulations into two populations: stars with masses $M_* \leq 1.9\ M_\odot$, and stars with masses $M_* > 1.9\ M_\odot$. The reason for this mass limit is related to the photoevaporation mass loss calculation and further explained in section 2.2. This mass separation is for photoevaporation purposes only and does not influence the dynamical evolution of the stars. All stars with masses $M_* \leq 1.9\ M_\odot$ are surrounded by a circumstellar disc, while stars with higher masses have no discs and are considered only as generating ionizing radiation. Massive stars are subject to stellar evolution, implemented using the code SeBa (Portegies Zwart & Verbunt 1996; Toonen et al. 2012) through its AMUSE interface. Stars with discs do not undergo stellar evolution in the simulations.

The dynamical evolution of the clusters is implemented using the 4th-order N-body code ph4, incorporated in AMUSE.

Circumstellar discs are implemented using the Viscous Accretion disc Evolution Resource (VADER) developed by Krumholz & Forbes (2015). VADER models mass and angular momentum transport on a thin, axisymmetric disc. This allows us to take into consideration the viscous spreading of the discs. Each VADER disc in our simulations is composed of a grid of 100 logarithmically spaced cells between 0.05 and 2000 au. The discs have a turbulence parameter of $\alpha = 5 \times 10^{-3}$.

The initial disc column density follows the standard disc profile by Lynden-Bell & Pringle (1974), with characteristic radius $r_c \approx r_d$ (Anderson et al. 2013):

$$\Sigma(r, t = 0) \approx \frac{m_d}{2\pi r_d \left(1 - e^{-1}\right)} \frac{\exp(-r/r_d)}{r} \quad (1)$$

where r_d and m_d are the initial radius and mass of the disc, respectively, and Σ_0 is a normalization constant. To define a disc radius we set the column density outside r_d to a negligible value $\Sigma_{\rm edge} = 10^{-12}\ {\rm g\,cm^{-2}}$.

2.2 External photoevaporation

External photoevaporation is dominated by far-ultraviolet (FUV) photons (Armitage 2000; Adams et al. 2004; Gorti

[1] `http://amusecode.github.io`
[2] `http://github.com/franciscaconcha/public-photoevap`

& Hollenbach 2009). To model the FUV radiation from the massive stars we pre-compute a relation between stellar mass and FUV luminosity using the UVBLUE spectral library (RodriguezâĂŘMerino et al. 2005). The obtained FUV luminosity fit is shown in Figure 2 of Paper I. During the simulations we use this fit to obtain the FUV luminosity of each massive star at every time step.

Mass loss due to external photoevaporation is calculated for each disc using the Far-ultraviolet Radiation Induced Evaporation of Discs (FRIED) grid (Haworth et al. 2018b). The FRIED grid provides a set of pre-calculated, external photoevaporation mass loss rates for discs immersed in radiation fields of varying intensity, from 10 G_0 to 10^4 G_0. The grid spans discs of mass $\sim 10^{-4}$ M_{Jup} to 10^2 M_{Jup}, radius from 1 au to 400 au, and host star mass from 0.05 $M_\odot$ to 1.9 $M_\odot$. To stay within the limits of the grid, we give all stars with masses $M_* \leq 1.9$ $M_\odot$ a circumstellar disc, and all stars with masses $M_* > 1.9$ $M_\odot$ are considered as only generating radiation.

We calculate the mass loss of every disc as follows. For each disc we begin by calculating its distance to every star of mass $M_* > 1.9$ $M_\odot$ and determining the total radiation that the disc receives from those stars. We do not consider extinction in this calculation. We then use this total radiation and the disc parameters to interpolate a mass loss rate $\dot{M}$ from the FRIED grid. This $\dot{M}$ is then used to calculate the total mass lost by the disc in the current time step. Assuming a constant mass loss rate over the time step, the mass is removed from the outer regions of the disc: we advance over the disc cells starting from the outside removing mass from each, until the corresponding amount of mass has been removed. Through this process, mass loss due to photoevaporation results in a decrease of disc mass and disc radius.

In some cases a massive star gets close enough to a disc to enter a photoevaporation regime dominated by extreme ultraviolet (EUV) radiation. We define a distance limit for this case following Johnstone et al. (1998):

$$d_{min} \simeq 5 \times 10^{17} \left(\frac{\epsilon^2}{f_r \Phi_{49}} \right)^{-1/2} r_{d_{14}}^{1/2} \text{ cm} \quad (2)$$

where f_r is the fraction of EUV photons absorbed in the ionizing flow, $\Phi_{49} = \frac{\Phi_i}{10^{49}} s^{-1}$ is the EUV photon luminosity of the source, and ϵ is a dimensionless normalizing parameter. The factor $\left(\frac{\epsilon^2}{f_r \Phi_{49}} \right)^{1/2} \approx 4$, and $r_{d_{14}} = \frac{r_d}{10^{14} cm}$ with r_d the disc radius.When the distance d between a disc and a massive star is $d < d_{min}$, EUV photons dominate the radiation and the mass loss is calculated as:

$$\dot{M}_{EUV} = 2.0 \times 10^{-9} \frac{(1+x)^2}{x} \epsilon r_{d_{14}} M_\odot \text{ yr}^{-1} \quad (3)$$

with $x \approx 1.5$ and $\epsilon \approx 3$ (Johnstone et al. 1998).

We consider a disc as dispersed when it has lost 99% of its initial mass or when its mean column density is lower than 1 g cm^{-2}.

Model name	R_{vir} [pc]	$\overline{M}_{M_*>1.9M_\odot}$ [$M_\odot$]	$\overline{N}_{*B}$	$\overline{N}_{*O}$
R0.1	0.1	$6.61^{+57.18}_{-7.57}$	23.5 ± 1.1	2.2 ± 1.1
R0.3	0.3	$6.62^{+81.98}_{-7.07}$	22.5 ± 2.8	2.5 ± 0.5
R0.5	0.5	$5.22^{+53.54}_{-4.41}$	25.1 ± 2.5	1.8 ± 1.1
R1.0	1.0	$5.61^{+41.72}_{-5.56}$	22.0 ± 3.0	1.8 ± 0.1
R2.5	2.5	$5.94^{+46.09}_{-5.06}$	23.8 ± 7.8	1.8 ± 1.2
R5.0	5.0	$6.37^{+76.43}_{-5.24}$	25.2 ± 4.3	2.5 ± 1.5

Table 1. Simulation models. First column: model name. Second column: initial virial radius, in parsec. Third column: mean mass of radiating stars ($M_* > 1.9 M_\odot$), in $M_\odot$. Fourth column: mean number of B type stars. Fifth column: mean number of O type stars. All means are calculated over 6 runs for each model.

2.3 Initial conditions

2.3.1 Star clusters

We simulate clusters with 10^3 stars and initial virial radii of 0.1, 0.3, 0.5, 1.0, 2.5, and 5.0 pc. Stars are initially distributed in a Plummer sphere (Plummer 1911). Stellar masses are drawn from a random Kroupa mass distribution (Kroupa 2001) with upper limit 100 $M_\odot$. All models start in virial equilibrium (virial ratio $Q = 0.5$). No primordial mass segregation, binaries, or higher multiplicity systems are considered.

In Table 1 we present the models used for this work. The mean number of stars with discs in each simulation is 974.7 ± 1.7. The mean mass of the stars with discs is $0.23^{+1.66}_{-0.22} M_\odot$. The mean number of stars generating UV radiation is 25.3 ± 1.7. The third column of Table 1 shows the mass ranges spanned by these stars.

We evolve each cluster for 2.0 Myr. We run each model 6 times, with a different random seed for the mass function and the initial stellar positions and velocities.

2.3.2 Circumstellar discs

Observations of resolved circumstellar discs suggest they are generally compact, with radii around 20 to 50 au (Trapman et al. 2020; Tobin et al. 2020). The initial radii of the discs in our simulations are given by:

$$R_d(t=0) = R' \left(\frac{M_*}{M_\odot} \right)^{0.5}, \quad (4)$$

where R' is a constant. We choose $R' = 30$ au, which yields an initial disc radii distribution between ~ 5 au and ~ 40 au.

Initial discs masses are defined as:

$$M_d(t=0) = 0.1 M_* \quad (5)$$

where M_* is the mass of the host star.

2.4 Model caveats

Our model is an approximation of the physical processes going on inside star-forming regions, in particular with regards

to external photoevaporation. There are quite a number of assumptions in our simulations which we justify based on previous theoretical work and observations. Below we discuss processes and parameters that have been overlooked and that have implications for our final results.

Star-forming regions are not only rich in stars but also in gas, which can linger for several million years (Portegies Zwart et al. 2010). Intracluster gas could influence our results in two main ways: first, the presence of gas and its subsequent expulsion in time affect the virial equilibrium and thus the dynamics of the star clusters. Second, gas can absorb some of the FUV radiation coming from bright stars, effectively protecting the discs from external photoevaporation and allowing them to live for longer (Winter et al. 2019a; Ali & Harries 2019; van Terwisga et al. 2020), and thus giving more time to the planet formation process to occur.

Another parameter which can alter the amount of radiation received by each disc is its inclination. Depending on its orientation, a disc can be irradiated by a nearby star face on, edge on, or a position in between. This can generate a discrepancy of mass loss in different regions of the disc. We do not give the discs in our model a particular orientation, but consider the effect of inclination averaged out as we take into account radiation coming from massive stars in different directions.

Internal photoevaporation, the process in which X-Ray and UV photons coming from the host star itself lead to mass loss, is also not included in these simulations. Internal photoevaporation can drive mass loss in the inner regions of the discs ($\sim 1-10$ au and 30 au, Gorti et al. 2009; Gorti & Hollenbach 2009) and even in outer regions under certain conditions (Owen et al. 2010; Font et al. 2004). However, external photoevaporation is arguably the dominant process in regions > 10 au (Hollenbach et al. 2000; Fatuzzo & Adams 2008). Our approximation of external photoevaporation removing mass from the outer regions of the disc only is also idealized, since while internal photoevaporation seems to clear the disc at specific radii, FUV photons coming from external sources can heat and evaporate mass from the whole disc surface (Adams et al. 2004).

The FRIED grid was constructed using a 1-dimensional disc model, but later simulations by Haworth & Clarke (2019) show that mass loss rates can increase up to a factor of 3.7 when considering 2-dimensional discs. It is likely then that the mass losses used in this work are only a lower limit for the effects of external photoevaporation.

Regarding disc masses, it is generally accepted that a 1:100 dust:gas mass ratio defines the composition of circumstellar discs. However, several authors have pointed out that this value might change across discs and in time (Williams & Best 2014; Manara et al. 2020). This can lead to observed disc dust masses being greatly underestimated (Manara et al. 2018). New models of externally irradiated, evaporating discs by Haworth et al. (2018a) show that considering grain growth can lead to less dust being lost through external photoevaporation, and thus to the dust:gas ratio increasing in time. A more careful implementation of the separate dust and gas components in a disc can help to overcome this problem.

The distribution of stars in a Plummer sphere is an idealized geometry. Star-forming regions have complex configurations and can present fractal structures, filaments, and other regions of increased surface density. The simulations carried out for this work represent only local densities, but for improved analyses of disc survival in star-forming regions it is important to consider different spatial distributions.

3 RESULTS

In Figure 1 we show the evolution of several stars and their corresponding circumstellar discs. These particular tracks are taken from one of the realisations of model R1.0. We show seven stars with discs as they move through the cluster. Black crosses mark the position of each star at the beginning of the simulation, and the label next to each shows the mass of the star. The sizes of the coloured circles in the stellar tracks are proportional to the disc radii, and their colour indicates the total disc mass. Red crosses, where present, show the moment when the disc is dispersed. The black thin lines that follow a red cross indicate the continuation of the orbit of the star, which keeps moving through the cluster after its disc has been evaporated. The trajectories of some massive, radiating stars are shown in thin blue lines. The solid and dashed circles in the background show the core radius and half mass radius of the cluster, respectively, at $t = 0.0$ Myr. A disc around a 0.37 $M_\odot$ star survives all through the simulation. A 0.14 $M_\odot$ star initially near the centre keeps its disc until around halfway through the simulation. A very low mass star, 0.06 $M_\odot$, loses its disc very quickly even if located in the periphery of the cluster. While our simulations are three-dimensional, in this illustrative figure we show a two-dimensional projection of the location of the stars.

3.1 Disc fractions and lifetimes

We define the disc fraction as the number of stars with discs over the total number of stars in each cluster at a certain moment. In Figure 2 we show disc fractions in time for the different models. The disc fraction at $t = 0.0$ Myr is less than 1.0, but never below 0.9, because we are calculating the fraction over all stars in each region, including the massive stars which do not have circumstellar discs. Final disc fractions decrease with increasing stellar number density. The R0.1 and R0.3 models show a very similar evolution, meaning that the density of the R0.3 model is a higher limit for the effects of external photoevaporation in destroying discs in such simulations. The R5.0 model has a final disc fraction of $\sim 45\%$, in contrast to $\sim 10\%$ for the R0.1 and R0.3 models.

A large drop in the number of stars with discs before 0.2 Myr is observed in models R0.1 and R0.3. Similar behaviour was obtained in the simulations performed in Paper I. This drop is related to discs around very low mass stars being dispersed rapidly once the simulation begins and external photoevaporation is 'turned on'. This drop can be seen in all the curves, but it becomes less pronounced for lower densities.

In Figure 3 we show disc fractions separated in terms of the mass of their host stars: low mass stars ($M_* \leq 0.5 M_\odot$) in the top panel and high mass stars ($0.5 M_\odot < M_* \leq 1.9 M_\odot$) in the bottom panel. The disc fraction for high mass stars stays constant through time for the R1.0, R2.5, and R5.0 models.

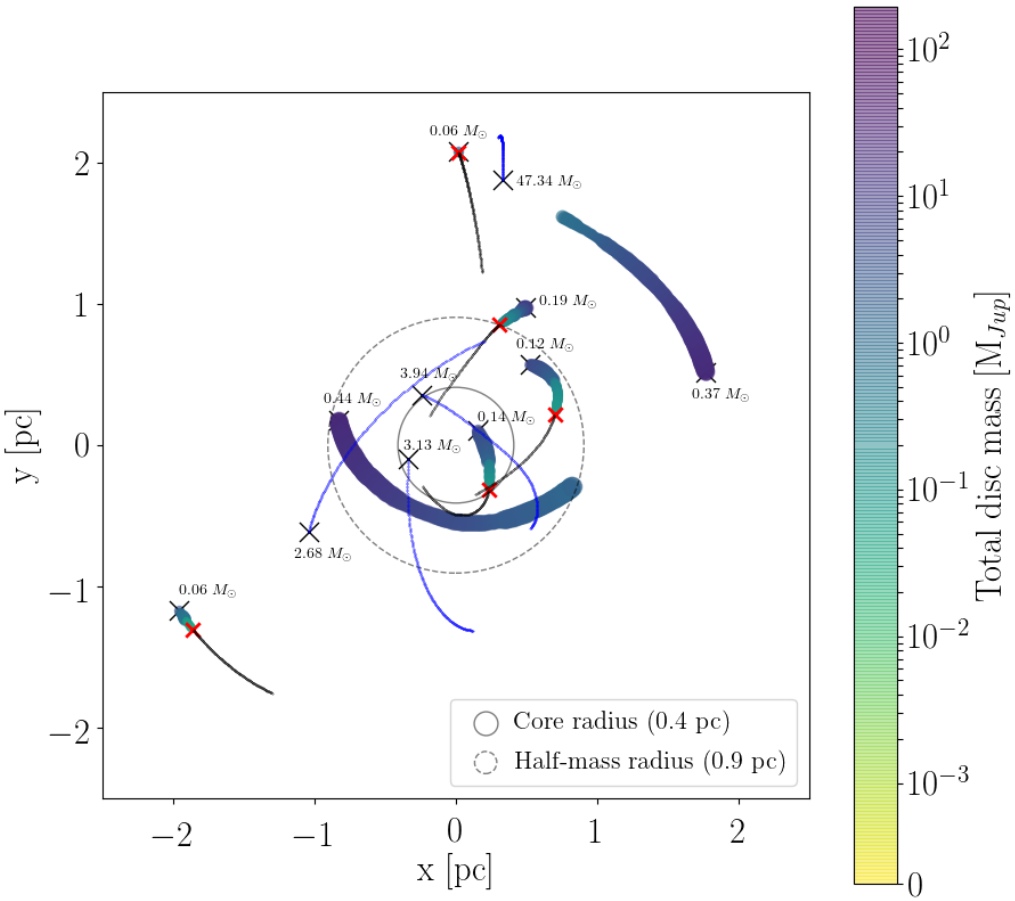

Figure 1. Example of cluster evolution for a realisation of the R1.0 model. Black crosses mark the position of the stars at the beginning of the simulation, and the label next to them shows the stellar mass. The sizes of the large, coloured points are proportional to the disc radii, and their colour indicates the total disc mass. The red crosses, when present, show the moment when a disc is dispersed. The thin black lines that follow a red cross indicate the continuing orbit of the star, which keeps moving through the region after its disc has been evaporated. The trajectories of some massive, radiating stars are shown in thin blue lines.

These discs lose mass but not enough to be completely evaporated, except for a slight decrease near the end for the R1.0 model. In the R0.1, R0.3, and R0.5 models, however, starting around 1.0 Myr even massive discs get destroyed.

In Figure 4 we show the mean FUV radiation field in time for the different models. There is a difference of several orders of magnitude between the mean radiation in the dense models and in the sparse models. While these curves show the mean value of radiation received by all discs at a point in time, it gives some insight regarding the mass loss process. In the sparser models an important part of photoevaporation mass loss occurs in 'bursts' in time. In the denser models the FUV radiation is consistently higher, but the curves are also less continuous. This reflects the fact that in those regions photoevaporation is not dominated by a few, very massive stars moving through the cluster, but by the sum of the radiation of all stars, which stay continuously closer to the discs than in the sparser regions.

In Table 2 we present the mean disc lifetimes and disc half-life for each model, averaged over 6 runs. Disc lifetimes are calculated as a mean of the times when a disc is completely dispersed in the simulations, following the dispersion criteria explained in section 2.2. It is important to mention that this mean is calculated only considering the discs that get dispersed within the 2.0 Myr spanned by the simulation, and the discs that survive would likely increase these values. Considering the resulting disc fractions, however, the obtained disc lifetimes are a good approximation. The disc half-life corresponds to the moment when half of the discs in a simulation have been dispersed. Both the disc lifetimes and the half-life increase with decreasing stellar density.

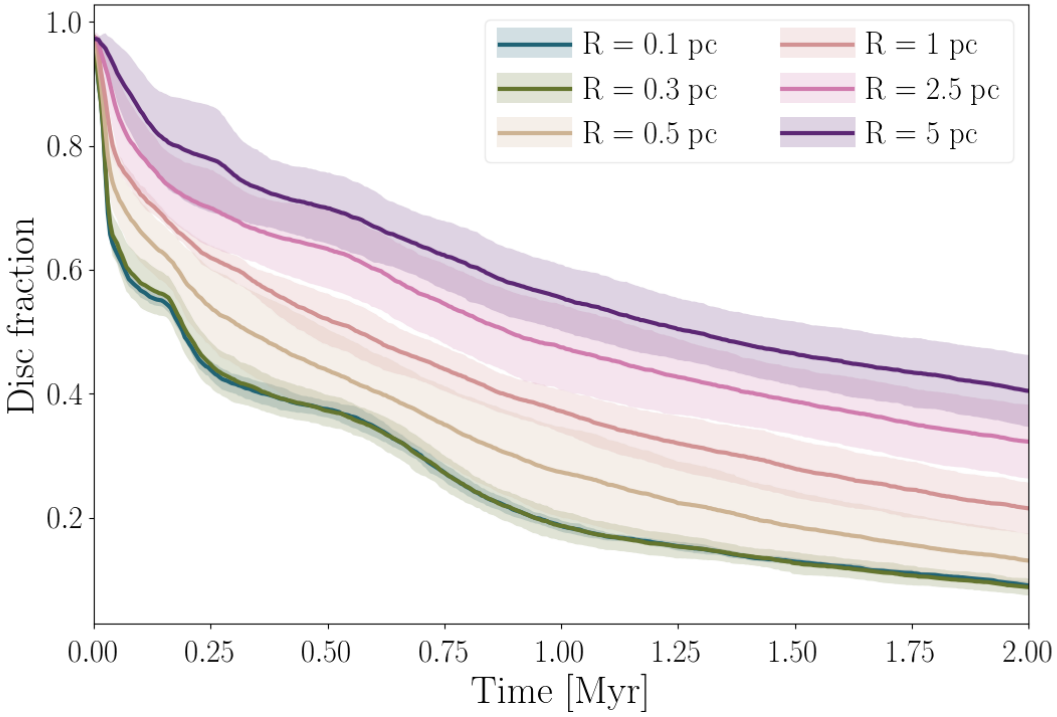

Figure 2. Disc fractions in time. The solid lines show the mean for 6 runs of each model, and the shaded areas represent the standard deviation.

Model name	Mean disc lifetime [Myr]	Discs half-life [Myr]
R0.1	0.38 ± 0.47	0.20 ± 0.01
R0.3	0.38 ± 0.47	0.22 ± 0.03
R0.5	0.47 ± 0.51	0.39 ± 0.16
R1.0	0.52 ± 0.55	0.59 ± 0.11
R2.5	0.59 ± 0.56	0.97 ± 0.25
R5.0	0.65 ± 0.55	1.42 ± 0.33

Table 2. Disc lifetimes and half-life for the different models. First column: model name. Second column: mean disc lifetimes for each model, in Myr. Third column: disc half-life in Myr, calculated as the moment when 50% of the discs in a simulation have been destroyed. The values are averaged over 6 runs for each model, and the errors represent the variations between runs.

3.2 Disc masses

In Figure 5 we show the evolution of the mean disc mass in time versus the local stellar number density. The local stellar number density is calculated for each star using the method described by Casertano & Hut (1985) with the 5 nearest neighbours. The binned mean disc mass is calculated using a sliding bin spanning 100 stars.

The thick dotted lines in Figure 5 show the mean disc mass at $t = 0.0$ Myr, and the thick solid lines at $t = 2.0$ Myr. The shaded areas around these lines represent the standard error. The thin lines in between show the evolution of the curve in 0.2 Myr intervals. The expansion of the clusters in time is reflected by the $t = 2.0$ Myr curves spanning larger density ranges than the $t = 0.0$ Myr curves. This effect is less pronounced in the R1.0, R2.5, and R5.0 models because they expand in a longer time scale. The slope of the final mean disc mass distribution increases with decreasing stellar density. This is related to the core density in each region, which is also decreasing: the curves in the R5.0 model are several orders of magnitude lower, in terms of density, than the R0.1 model. The R0.1 model has a distribution of disc masses such that the most massive discs are found further away from the centre, with differences of about one order of magnitude between the discs located in the centre and in the outskirts of the cluster. In the R5.0 model, the mass difference between discs in different locations is much smaller, and the disc masses are of the same order of magnitude through all the density range.

In Figure 6 we show the mean dust mass of the discs versus the projected local density. We use a 1:100 dust:gas mass radio to determine the dust mass of our discs. We calculate the density in the same way as in Figure 5, but projecting the distances between stars to two dimensions. This allows us to compare disc dust masses in our simulations to observed disc populations. The blue diamonds show points of average disc dust mass versus local density of young stellar objects for the Lupus clouds (Ansdell et al. 2016, 2018), the Orion Nebula Cluster (ONC, Mann et al. 2014; Eisner et al. 2018), the Orion Molecular Cloud-2 (OMC-2, van Terwisga et al. 2019), Taurus (Andrews et al. 2013), and NGC 2024 East and West (Getman et al. 2014), as labelled. We

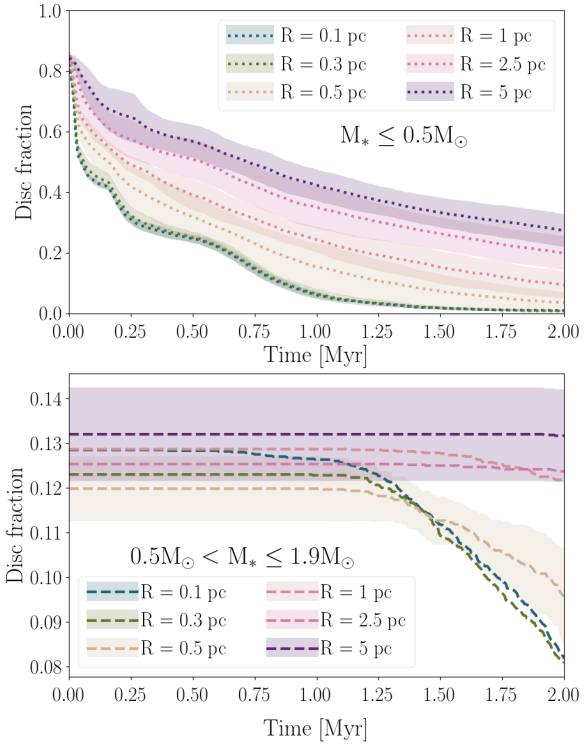

Figure 3. Disc fractions in time separated by stellar mass. The top panel shows disc fractions for low mass stars ($M_* \leq 0.5M_\odot$) and the bottom panel for high mass stars ($0.5M_\odot < M_* \leq 1.9M_\odot$). The lines show the mean for 6 runs of each model, and the shaded areas represent the standard deviation. For clarity, in the bottom panel we plot the standard deviation only for the R0.5 and R5.0 models, but the rest of the models have deviations of similar magnitude.

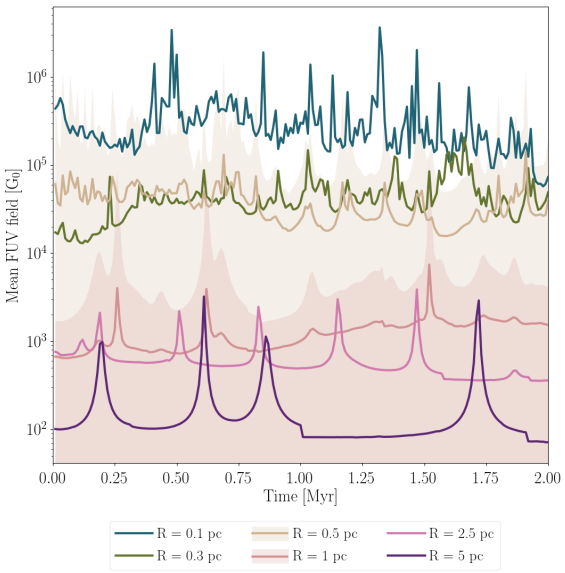

Figure 4. Mean FUV radiation field received by the circumstellar discs in time. The solid lines show the mean for 6 runs of each model, and the shaded areas represent the standard deviation. For clarity we plot the standard deviation only for the R0.5 and R1.0 models, but the rest of the models have deviations of similar magnitude.

do not look to reproduce the observed disc distributions in those regions or to determine if one of our models fits the observed disc masses. These observations span regions of different stellar ages and populations, as well as different spatial distributions. A direct comparison between them, as well as comparing them to our models, is not straightforward to make. However, these observational points are helpful for us as they indicate whether the trends that we see in our simulations have support in observed disc distributions at regions of different densities.

Figure 6 shows a break in disc masses around a local density of 100 stars pc^{-2}. The slope of the disc mass distribution changes around that point for all models, except R5.0. In models R2.5 and R1 we see the slope of the distributions increasing as we move towards higher densities. For the R0.1, R0.3, and R0.5 models, we see disc mass distributions stay relatively constant for densities lower than 100 stars pc^{-2}, and for higher densities we see a negative slope. The difference in masses between 100 stars pc^{-2} and 10^4 stars pc^2 is about one order of magnitude. A similar effect can be seen in the observational points, except for NGC 2024 East. This behaviour suggests that 100 stars pc^{-2} is a critical density for determining disc masses.

The average disc dust masses of the observations are calculated by fitting a log-normal distribution on the masses. The local density for each point is calculated using the five nearest neighbours method. Lupus data is an average for all the clouds, using the complete list of Class II sources in Ansdell et al. (2016) and Ansdell et al. (2018). It is important to note that the Lupus III cloud dominates the signal for that particular region, because it has the largest population of Class II sources. For the OMC-2 the data comes from van Terwisga et al. (2019), who use the source catalog from Megeath et al. (2012) assuming completeness. ONC data comes from Megeath et al. (2016), including completeness corrections.

In the OMC-2 and ONC regions, observations sample two different density regimes in the same cloud, relatively close together in space. Therefore, the conditions in our models most closely resemble the properties of the disks that were sampled by the observations, and we can interpret them as different density bins along a single model. It is immediately apparent that both the gradient of average disk mass with density as well as the average disk masses themselves resemble the models closely. Given the considerable uncertainties in extracting disk masses from millimeter-continuum observations (see, for instance, the discussion in Eisner et al. (2018)) the similarity in the gradients suggests that our models are successful at capturing the general behaviour of external photoevaporation.

In NGC 2024, Getman et al. (2014) find evidence for an age gradient of young stars, which van Terwisga et al. (2020) suggest as an explanation for the large difference in mean disk masses in NGC 2024 East and NGC 2024 West. In NGC 2024, the western part is the older and resembles the ONC in age and conditions, while the eastern disk population has a lower average age. We represent this difference in the figure by making NGC 2024 East in a different shade. It is interesting to note that Getman et al. (2014) also suggest such an age gradient in the ONC, albeit less pronounced.

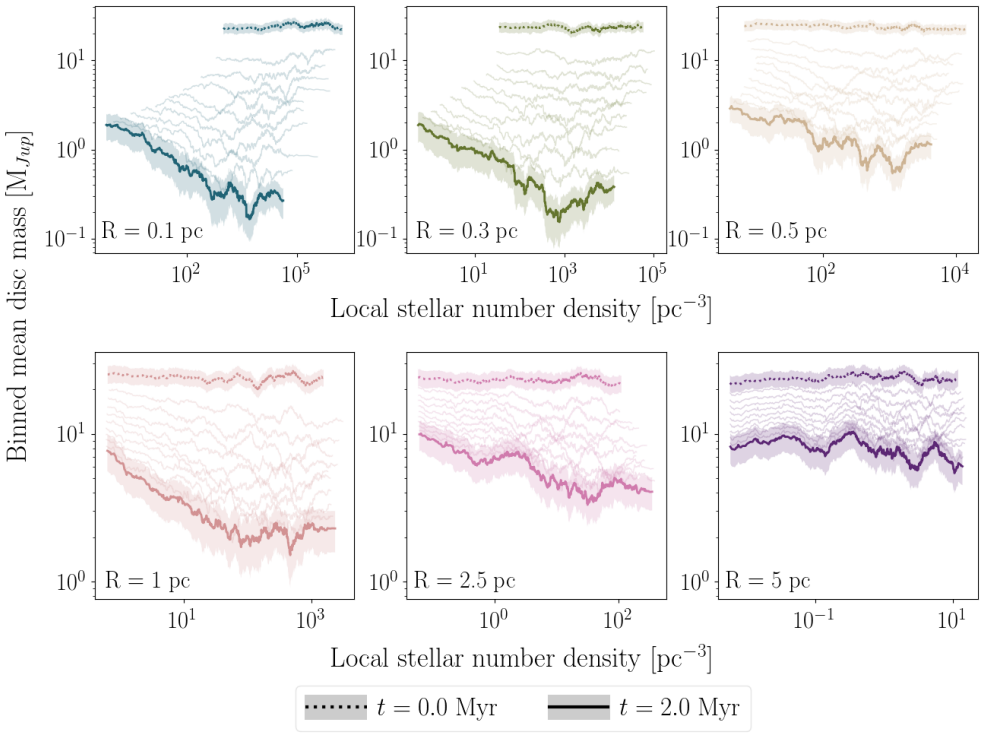

Figure 5. Binned mean disc mass versus local stellar number density. The mean mass is calculated using a moving bin spanning 100 stars. The local density is calculated for each star as explained in section 3.2. The dotted lines thick represent the binned mean disc mass at t = 0.0 Myr and the solid thick lines at t = 2.0 Myr. The shaded areas show the standard error. The thin lines represent the binned mean at 0.2 Myr intervals.

Comparing these models to the observations, we see that the NGC 2024 West data lie closely to those of the ONC, while the data for the eastern subpopulation occupy region of average disk mass and local stellar density space which is more consistent with a younger, compact population of stars, in agreement with this hypothesis.

Lupus and Taurus disks, on the other hand, sample a much more heterogeneous part of parameter space in terms of initial densities. Our models do not closely resemble the conditions under which the stars in these samples formed (see, for instance, Roccatagliata et al. (2020)). However, the result that when the average stellar number density is low enough (below ~100 stars pc^{-2}) the average disc masses are similar at similar ages does seem to apply to these star-forming regions, even though this is a part of parameter space we do not explore.

In Figure 7 we show the cumulative distributions of disc dust masses at t = 2.0 Myr. For the R0.1, R0.3, and R0.5 models almost all discs have dust masses lower than 100 $M_\oplus$. In the R5.0 model, both very low dust mass (~ 0.1 $M_\oplus$) and high dust mass (~ 500 $M_\oplus$) discs are present. In Figure 8 we present the same cumulative distributions of disc dust mass, but separated in low mass stars and high mass stars. The mass distributions of discs around high mass stars are directly related to the density of each region: the R5.0 model has the higher disc masses, and this number decreases as the models move towards higher densities with R0.1 and R0.3 having the lowest mass distributions. For low mass stars, however, the relation with disc mass and density is not so direct. This same effect was previously displayed in Figure 3 and it shows that discs around low mass stars are very sensitive to external photoevaporation. This effect is also related to our model definitions, since discs around low mass stars are initially less massive by construction.

The effects of photoevaporation in our models can be seen in the decreasing number of surviving discs and in the mass distributions of the discs that survive until the end of the simulations. Models where the radiation is more intense have fewer discs by the end of the runs, and these discs are less massive than in sparser regions.

In Figures 9 and 10 we show the total disc mass versus local number density. We plot all discs in all the 6 realisations of each model. The colour of each point represents the initial local density of the host star, and the sizes of the points are proportional to the disc radius. In time, the discs move towards the left and bottom of the panels. The movement to the left reflects the dynamical expansion of each cluster. The movement to the bottom reflects the diminishing disc masses with time. In these figures larger discs end up in the left side of the panels. This shows that being in lower density regions allows discs to expand viscously without being greatly truncated or suffering an important mass loss. It can also be seen that, particularly in the R1.0, R2.5, and R5.0, models, the discs in the outer regions of the clusters remain close to where they formed, their local density staying mostly constant during the time spanned by the simulations. These figures show that, in our simulations,

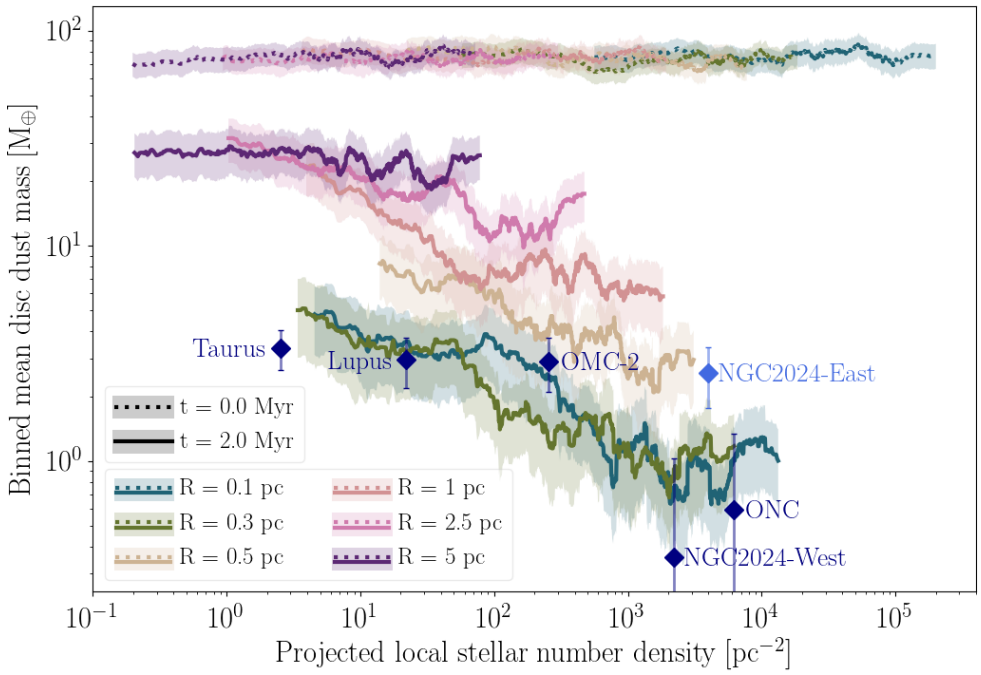

Figure 6. Binned mean disc mass versus local stellar number density, projected in two dimensions. The mean mass is calculated using a moving bin spanning 100 stars. The local density is calculated for each star as explained in section 3.2, but projecting the distances between stars into two dimensions. The dotted lines thick represent the binned mean disc mass at t = 0.0 Myr and the solid thick lines at t = 2.0 Myr. The shaded areas show the standard error. Diamonds show average disc dust masses and local stellar densities for several observed regions. The different color used for NGC 2024 symbolises the different age of the region.

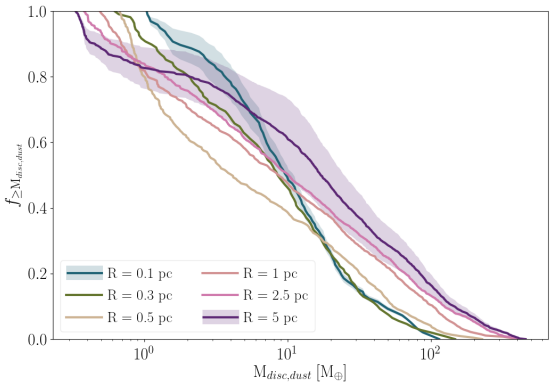

Figure 7. Cumulative distributions of disc dust mass at t = 2.0 Myr. Shaded areas represent the standard deviation. For clarity, this is shown only for the R0.1 and R5.0 models, but the other models have deviations of similar magnitude.

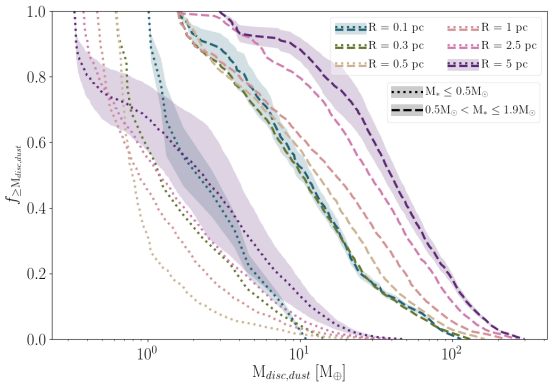

Figure 8. Cumulative distributions of disc dust mass separated in low mass stars ($M_* \leq 0.5 M_\odot$) and high mass stars ($0.5 M_\odot < M_* \leq 1.9 M_\odot$). The dotted and dashed lines represent the distribution of low mass stars and high mass stars, respectively, at t = 2.0 Myr, and the shaded areas represent the standard deviation. For clarity, this is shown only for the R5.0 model, but the other models have deviations of similar magnitude.

massive and large discs are more likely to be found in regions of low stellar density.

4 DISCUSSION

In the simulations performed for this work, external photoevaporation is effective in destroying the majority number of discs within 2.0 Myr of evolution. The initial stellar density of each region affects the fraction of surviving discs, as well as their final mass distributions. In all models, except for R5.0, half of the discs are destroyed before 1.0 Myr of cluster evolution. The mean disc lifetimes, disc half-life, mean

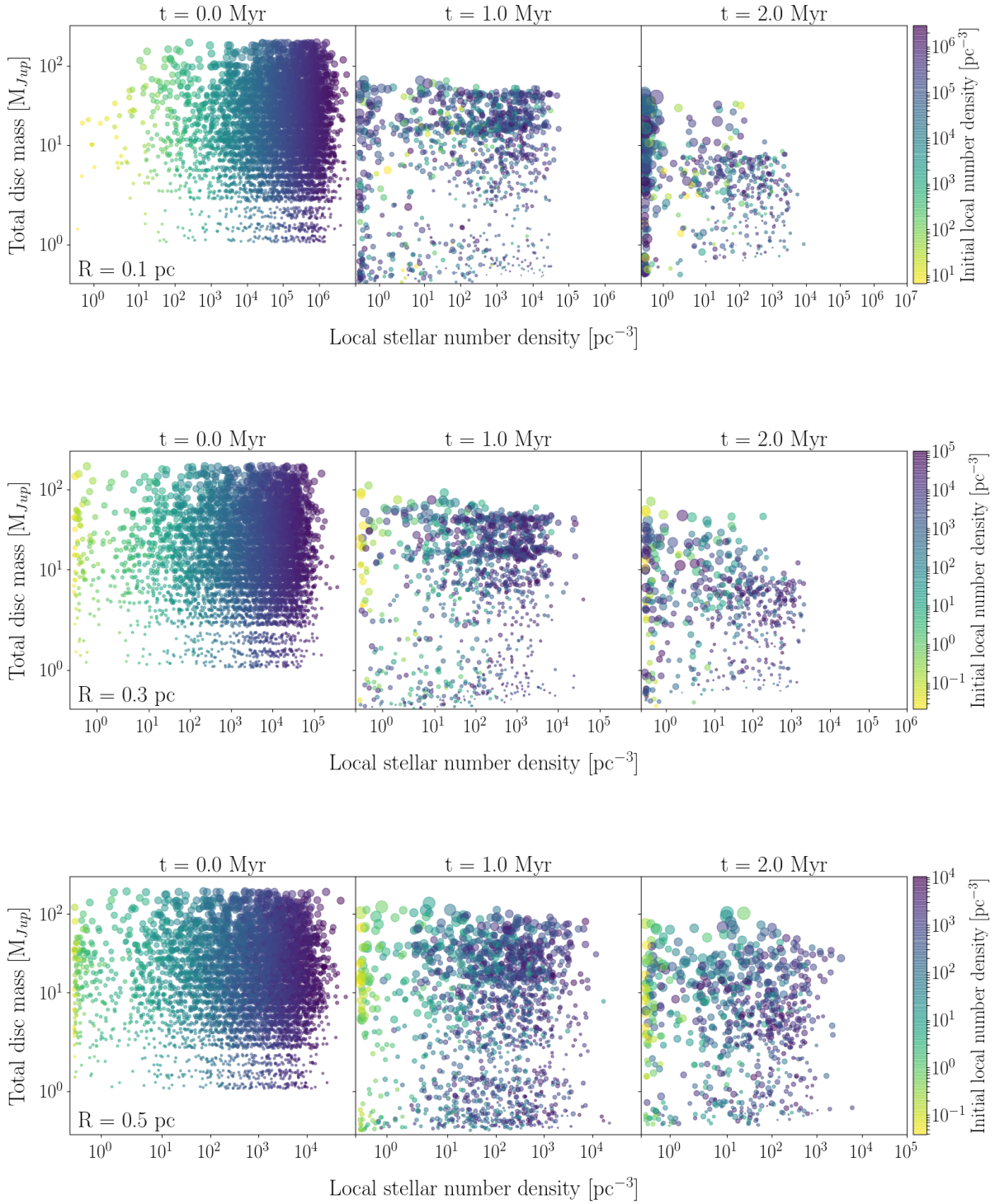

Figure 9. Total disc mass versus local stellar number density for the R0.1 (top), R0.3 (middle), and R0.5 (bottom) models at $t = 0.0$ Myr (left panels), $t = 1.0$ Myr (centre panels), and $t = 0.0$ Myr (right panels). The plots show all discs in all 6 realisations of each model. The colour of each point represents the initial local density of the host star, and the sizes of the points are proportional to the disc radius.

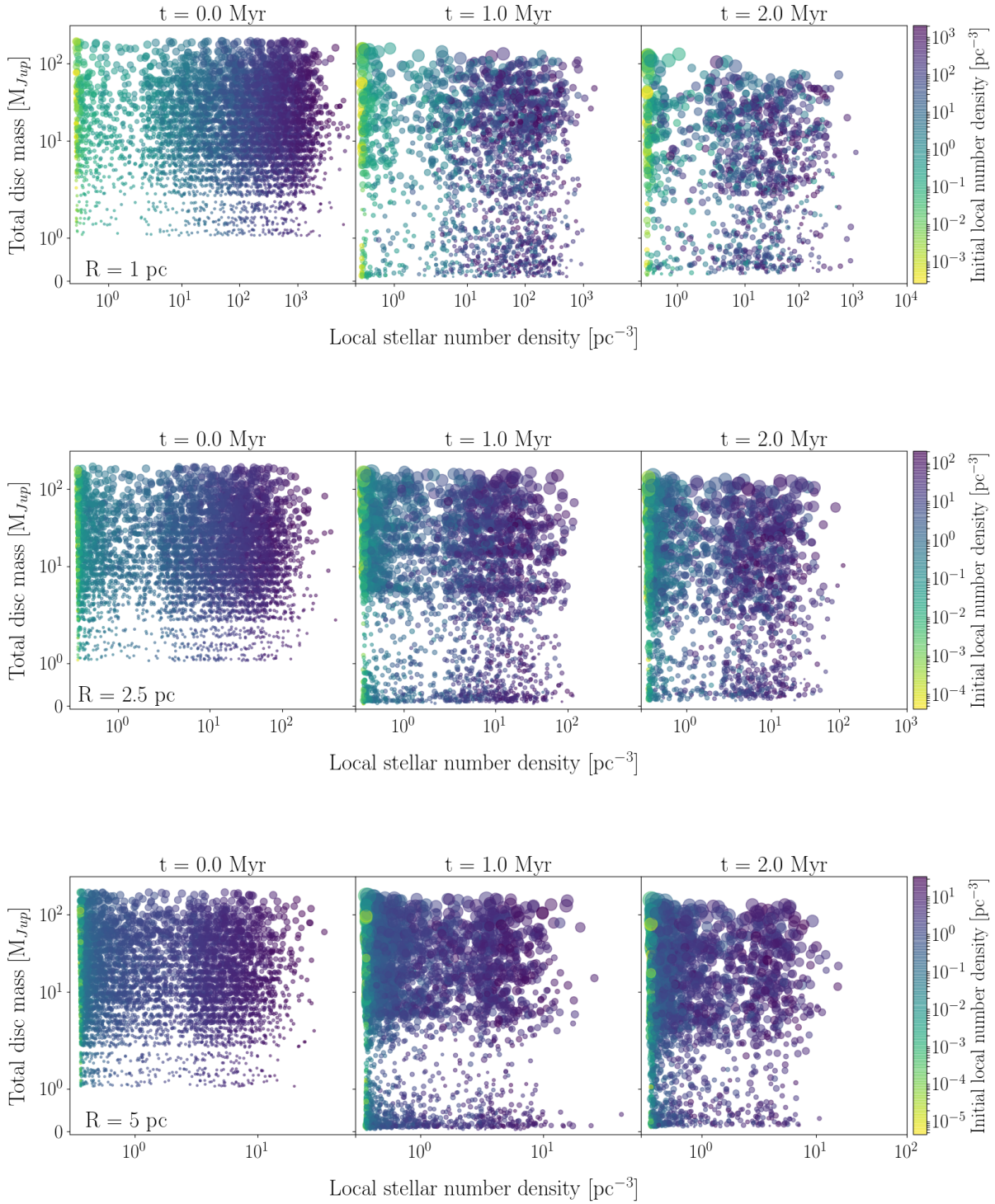

Figure 10. Total disc mass versus local stellar number density for the R1.0 (top), R2.5 (middle), and R5.0 (bottom) models at t = 0.0 Myr (left panels), t = 1.0 Myr (centre panels), and t = 0.0 Myr (right panels). The plots show all discs in all 6 realisations of each model. The colour of each point represents the initial local density of the host star, and the sizes of the points are proportional to the disc radius.

disc masses, and number of discs at the end of the simulation all decrease with increasing stellar density. The effects of stellar density over disc mass are not only apparent when comparing the different models, but also within the models themselves. A break in the disc masses is seen around 100 stars pc^{-2} in particular for the R0.1 and R0.3 models, with masses dropping about one order of magnitude between 100 stars pc^{-2} and 10^4 stars pc^{-2}.

Our results suggest that, considering circumstellar discs as the precursors of planetary systems, the amount of material available to form planets decreases rapidly in high density environments. For planets to form in regions like the ones simulated in this work, planet formation should already be underway before 1.0 Myr and even earlier. Our theoretical results are in agreement with other models of disc dispersal by external photoevaporation, such as the work by Winter et al. (2019b) and Nicholson et al. (2019). Winter et al. (2019b) find that 90% of circumstellar discs are destroyed by external photoevaporation within 1.0 Myr in a region comparable to the Central Molecular Zone of the Milky Way, and that the effects of photoevaporation are particularly destructive for discs around low mass stars ($M_* < 0.3 M_\odot$). For regions similar to the solar neighborhood (surface density Σ_0 = 12 $M_\odot$ pc^{-2}) they find a mean dispersal timescale of $\sim$ 3.0 Myr.

There are observational indications that planet formation starts shortly after stars form. The 'missing-mass problem' refers to the discrepancy between measured protoplanetary disc masses and the masses of observed planetary systems. Even the most massive discs do not appear to have enough mass in solids to form the rocky planetary systems discovered so far (Greaves & Rice 2010; Najita & Kenyon 2014; Manara et al. 2018). Several possible solutions for this problem have been proposed, including adjusting the conversion factors between millimetre flux to disc dust mass. Greaves & Rice (2010) propose that this is not enough to fix the discrepancy in masses, and in turn they propose the idea of planet formation starting early on, even within the first 0.1 Myr since star formation.

Figure 8 shows that, for low mass stars, the effects of external photoevaporation are heterogeneous through all models, and more closely dependent on stellar density for high mass stars. Discs around low mass stars seem to be destroyed in similar proportions across all regions, except for models R2.5 and R5.0 where fractions of discs around low mass stars drop only by half by the end of the simulations (Figure 3). Model R5.0 is sparse enough to keep both low mass ($M_{disc,dust} \sim 0.1 M_\oplus$) and high mass ($M_{disc,dust} \sim 50 M_\oplus$) discs around low mass stars. It is likely that low mass discs that survive in such an environment move away from the cluster centre during its dynamical evolution.

Most of the surviving discs in our simulations are around massive stars (0.5 $M_\odot$ to 1.9 $M_\odot$). A big factor in this is simply the construction of our models, where initial disc mass is proportional to stellar mass. Figure 3, however, shows that drops of around 50% in fractions of discs around high mass stars are still present in high density regions. Following equations 4 and 5, these discs around massive stars had initial radii between $\sim$ 21 au and $\sim$ 41 au and initial masses in the $\sim$ 52 M_{Jup} to $\sim$ 199 M_{Jup} range. Using a 1:100 dust:gas mass ratio we can interpret the initial dust masses of those discs as being between $\sim$ 166 $M_\oplus$ and $\sim 6.37 \times 10^4$ $M_\oplus$. As can be seen in Figure 7, in the R5.0 model this results on disc dust mass distributions between $\sim$ 5 $M_\oplus$ and $\sim$ 120 $M_\oplus$. For the R0.1 model the final dust masses are between $\sim$ 5 $M_\oplus$ and $\sim$ 100 $M_\oplus$, but with around 20% fewer discs.

Ansdell et al. (2016) suggest that a reservoir of at least 10$M_\oplus$ is necessary to form rocky planets or the cores of gas giants. To be able to form gas giants, these cores should be formed before 1.0 Myr to ensure that there is enough gas available in the disc to form the planets. In the R5.0 model, over 90% of discs satisfy this condition, whereas in the R0.1 around 50% of discs do. For the R5.0 model, around 75% of discs around low mass stars satisfy this condition. Most of these discs, in all models, are around stars with masses $0.5 M_\odot < M_* \leq 1.9 M_\odot$.

We know, however, that planets do form around low mass stars. The host star of one of the most exciting planetary systems discovered so far, TRAPPIST-1, is an M-dwarf type star with a mass of 0.089$M_\odot$ (Gillon et al. 2017). Circumstellar discs have been detected around brown dwarfs in Lupus (Sanchis et al. 2020) and Ophiuchus (Testi et al. 2016). Discs around very low mass stars and brown dwarfs seem to follow the same evolutionary trends as discs around more massive stars, but their discs might be less massive to begin with (Sanchis et al. 2020). Beyond just discs, several planetary-mass companions have been detected orbiting brown dwarfs, in particular in the Taurus region (Todorov et al. 2010) and in the young, low mass TW Hydrae association (Chauvin et al. 2004). It is interesting to note that Todorov et al. (2010) estimate an age of $\sim$ 1.0 Myr for the detected companion. According to our results, it is likely for such a low mass disc to survive as long as it is immersed in low density regions, or regions without a lot of massive stars.

In our simulations, the largest and most massive discs are located in the sparser regions. Similar distributions have been observed in star-forming regions. While a decrease in disc fractions and disc masses is observed with age (e.g. in Upper Scorpio, Barenfeld et al. 2016), in general sparser regions such as Lupus, Taurus, or OMC-2 have larger dust masses than discs in dense regions such as the ONC or the Trapezium (Mann et al. 2014; Ansdell et al. 2016; Eisner et al. 2018; van Terwisga et al. 2019). In these regions, proximity to massive stars causes disc masses to diminish even for young discs.

From Figures 9 and 10 it can be seen that, at the end of the simulations, the largest and most massive discs are located in areas where the local stellar density is lower, for all simulation models. This implies that large, massive discs observed today either formed in low density regions or migrated to the outskirts of their birth locations fairly quickly. Discs born in the periphery of such regions have a much larger chance of surviving, and we could argue that the disc distributions seen in these low density regions are similar to primordial disc distributions as they are pretty much unperturbed by external photoevaporation.

According to both the observational and theoretical accounts of external photoevaporation, when measuring disc masses to estimate disc ages it is important to consider how the environment of a disc might have changed through time. A massive disc probably formed and spent all of its life in a low density environment, whereas a less massive disc lo-

cated in a sparse region might have been born closer to a bright star but managed to move away in time to survive. In either case, the density of the birth environment defines the chances of a disc for surviving and its final mass.

As mentioned in section 2.4, there are several physical mechanisms that are not considered in this work and that can affect our results. It is likely that we are overestimating the effects of external photoevaporation by not taking into account the presence of intracluster gas. Gas can have a dampening effect by absorbing FUV photons and protecting circumstellar discs from external photoevaporation (Winter et al. 2019a; Ali & Harries 2019; van Terwisga et al. 2020). Considering the presence of gas would likely extend the disc lifetimes and half-lives. Not taking into account the inclination of discs with respect to the radiating stars can also take us to overestimate the mass loss. On the other hand, there are internal processes not considered in this work which can quickly diminish the dust mass of circumstellar discs. Both internal photoevaporation and planet formation can lead to lower dust masses, as well as dust clearing at certain disc radii. Including these effects could also make a difference in the survival of discs around low and high mass stars. A more careful modelling of the dust evolution inside the discs is needed to quantify the effects of these processes.

5 CONCLUSIONS

We perform simulations of star clusters with 10^3 stars and initial virial radii 0.1, 0.3, 0.5, 1.0, 2.5, and 5.0 pc to span a range of different number densities. Stars with masses $M_* \leq 1.9 M_\odot$ are initially surrounded by a circumstellar disc, and stars with masses $M_* > 1.9 M_\odot$ do not have discs and are considered as only emitting UV radiation. Each cluster is evolved for 2.0 Myr, during which dynamical evolution and external photoevaporation take place. We can summarize our findings as follows:

1. External photoevaporation is efficient in destroying circumstellar discs quickly in all simulation models.
2. As some quantification, mean disc lifetimes range from 0.38 ± 0.47 Myr in the denser models ($R_{cluster}$ = [0.1, 0.3, 0.5] pc), to 0.65 ± 0.55 Myr for the sparser models ($R_{cluster}$ = [1.0, 2.5, 5.0] pc).
3. Disc half-life, the time that it takes for half of the discs to be destroyed in a simulation run, ranges from 0.20 ± 0.01 Myr in the denser models to 1.42 ± 0.33 Myr in the sparser models.
4. Disc lifetimes, disc half-lives, disc fractions, and disc masses decrease as the stellar density of the models increase.
5. For the final disc masses in the denser regions ($R_{cluster}$ = [0.1, 0.3, 0.5] pc) a local number density of 100 stars pc^{-2} defines a break in the distributions. There are no great variations in the masses of discs around stars in areas of lower densities. As the density increases beyond 100 stars pc^{-2}, the denser regions present a drop of almost an order of magnitude in disc masses.
6. Regions that are initially dense lead to a lower number of discs than in sparser regions, and the surviving discs are less massive. Sparse regions span a larger range of masses of the surviving discs.
7. By the end of our simulations the largest and most massive discs are found in the periphery of the clusters, in particular for the models with higher stellar densities.
8. The trends obtained in our simulations between disc mass and region density are well in agreement with dust mass measurements of discs in different observed regions: we compare our simulation results to masses of dusty young stellar objects in the Lupus clouds, the Orion Nebula Cluster, the Orion Molecular Cloud-2, Taurus, and NGC2024. While we do not seek to fit a model to these observations, the fact that we see the same trends in our simulations as in observations is helpful for further development of our models.

ACKNOWLEDGEMENTS

F.C.-R. would like to thank the Star formation and protoplanetary disc group at Leiden Observatory for helpful discussions and insights. This work was carried out on the Dutch national e-infrastructure with the support of SURF Cooperative. This work was performed using resources provided by the Academic Leiden Interdisciplinary Cluster Environment (ALICE). This paper makes use of the packages `numpy` (Van Der Walt et al. 2011), `scipy` (Virtanen et al. 2019), `matplotlib` (Hunter 2007), and `makecite` (Price-Whelan et al. 2018).

DATA AVAILABILITY

The data underlying this article are available at `http://github.com/franciscaconcha/public-photoevap`.

REFERENCES

Adams F. C., Hollenbach D., Laughlin G., Gorti U., 2004, ApJ, 611, 360
Ali A. A., Harries T. J., 2019, Monthly Notices of the Royal Astronomical Society, 487, 4890
Anderson K. R., Adams F. C., Calvet N., 2013, ApJ, 774, 9
Andrews S. M., Rosenfeld K. A., Kraus A. L., Wilner D. J., 2013, The Astrophysical Journal, 771, 129
Ansdell M., et al., 2016, ApJ, 828, 46
Ansdell M., Williams J. P., Manara C. F., Miotello A., Facchini S., van der Marel N., Testi L., van Dishoeck E. F., 2017, AJ, 153, 240
Ansdell M., et al., 2018, ApJ, 859, 21
Armitage P. J., 2000, Astronomy and Astrophysics, 362, 968
Barenfeld S. A., Carpenter J. M., Ricci L., Isella A., 2016, ApJ, 827, 142
Bhandare A., Pfalzner S., 2019, Computational Astrophysics and Cosmology, 6, 3
Casertano S., Hut P., 1985, The Astrophysical Journal, 298, 80
Chauvin G., Lagrange A.-M., Dumas C., Zuckerman B., Mouillet D., Song I., Beuzit J.-L., Lowrance P., 2004, Astronomy and Astrophysics, 425, L29
Close J. L., Pittard J. M., 2017, MNRAS, 469, 1117
Concha-Ramírez F., Wilhelm M. J. C., Portegies Zwart S., Haworth T. J., 2019, Monthly Notices of the Royal Astronomical Society, 490, 5678
Eisner J. A., et al., 2018, The Astrophysical Journal, 860, 77
Facchini S., Clarke C. J., Bisbas T. G., 2016, MNRAS, 457, 3593

Fang M., et al., 2012, A&A, 539, A119
Fatuzzo M., Adams F. C., 2008, ApJ, 675, 1361
Font A. S., McCarthy I. G., Johnstone D., Ballantyne D. R., 2004, The Astrophysical Journal, 607, 890
Getman K. V., Feigelson E. D., Kuhn M. A., 2014, The Astrophysical Journal, 787, 109
Gillon M., et al., 2017, Nature, 542, 456
Gorti U., Hollenbach D., 2009, The Astrophysical Journal, 690, 1539
Gorti U., Dullemond C. P., Hollenbach D., 2009, The Astrophysical Journal, 705, 1237âĂŞ1251
Greaves J. S., Rice W. K. M., 2010, MNRAS, 407, 1981
Guarcello M. G., et al., 2016, arXiv:1605.01773 [astro-ph]
Haworth T. J., Clarke C. J., 2019, Monthly Notices of the Royal Astronomical Society, 485, 3895
Haworth T. J., Owen J. E., 2020, arXiv:2001.05004 [astro-ph]
Haworth T. J., Facchini S., Clarke C. J., Mohanty S., 2018a, MNRAS, 475, 5460
Haworth T. J., Clarke C. J., Rahman W., Winter A. J., Facchini S., 2018b, MNRAS, 481, 452
Hollenbach D. J., Yorke H. W., Johnstone D., 2000, Protostars and Planets IV, p. 401
Hunter J. D., 2007, Computing in Science & Engineering, 9, 90
Johnstone D., Hollenbach D., Bally J., 1998, The Astrophysical Journal, 499, 758
Kim J. S., Clarke C. J., Fang M., Facchini S., 2016, The Astrophysical Journal, 826, L15
Kroupa P., 2001, MNRAS, 322, 231
Krumholz M. R., Forbes J. C., 2015, Astronomy and Computing, 11, 1
Lynden-Bell D., Pringle J. E., 1974, MNRAS, 168, 603
Manara C. F., Morbidelli A., Guillot T., 2018, Astronomy and Astrophysics, 618, L3
Manara C. F., et al., 2020, arXiv:2004.14232 [astro-ph]
Mann R. K., et al., 2014, ApJ, 784, 82
Megeath S. T., et al., 2012, The Astronomical Journal, 144, 192
Megeath S. T., et al., 2016, The Astronomical Journal, 151, 5
Najita J. R., Kenyon S. J., 2014, MNRAS, 445, 3315
Nicholson R. B., Parker R. J., Church R. P., Davies M. B., Fearon N. M., Walton S. R. J., 2019, arXiv:1902.11094 [astro-ph]
O'dell C. R., 1998, AJ, 115, 263
O'dell C. R., Wen Z., 1994, The Astrophysical Journal, 436, 194
Owen J. E., Ercolano B., Clarke C. J., Alexander R. D., 2010, Monthly Notices of the Royal Astronomical Society, 401, 1415
Pelupessy F. I., Portegies Zwart S., 2012, MNRAS, 420, 1503
Plummer H. C., 1911, MNRAS, 71, 460
Portegies Zwart S. F., 2016, MNRAS, 457, 313
Portegies Zwart S. F., Verbunt F., 1996, A&A, 309, 179
Portegies Zwart S., et al., 2009, New Astronomy, 14, 369
Portegies Zwart S. F., McMillan S. L. W., Gieles M., 2010, ARA&A, 48, 431
Portegies Zwart S., Pelupessy I., van Elteren A., Wijnen T. P. G., Lugaro M., 2018, A&A, 616, A85
Price-Whelan Mechev A., jumeroag 2018, Adrn/Makecite: V0.2, Zenodo, doi:10.5281/zenodo.1343299
Roccatagliata V., Franciosini E., Sacco G. G., Randich S., Sicilia-Aguilar A., 2020, Astronomy & Astrophysics
RodriguezâĂŘMerino L. H., Chavez M., Bertone E., Buzzoni A., 2005, ApJ, 626, 411
Sanchis E., et al., 2020, Astronomy and Astrophysics, 633, A114
Testi L., Natta A., Scholz A., Tazzari M., Ricci L., Monsalvo I. d. G., 2016, Astronomy & Astrophysics, 593, A111
Tobin J. J., et al., 2020, The Astrophysical Journal, 890, 130
Todorov K., Luhman K. L., McLeod K. K., 2010, The Astrophysical Journal, 714, L84
Toonen S., Nelemans G., Zwart S. P., 2012, A&A, 546, A70
Trapman L., Rosotti G., Bosman A. D., Hogerheijde M. R., van Dishoeck E. F., 2020, arXiv:2005.11330 [astro-ph]
Tychoniec Å., et al., 2020, arXiv:2006.02812 [astro-ph]
Van Der Walt S., Colbert S. C., Varoquaux G., 2011, preprint, p. arXiv:1102.1523
Vincke K., Breslau A., Pfalzner S., 2015, A&A, 577, A115
Virtanen P., et al., 2019, arXiv:1907.10121 [physics]
Wijnen T. P. G., Pols O. R., Pelupessy F. I., Portegies Zwart S., 2016, A&A, 594, A30
Wijnen T. P. G., Pols O. R., Pelupessy F. I., Portegies Zwart S., 2017, A&A, 602, A52
Williams J. P., 2012, Meteoritics and Planetary Science, 47, 1915
Williams J. P., Best W. M. J., 2014, The Astrophysical Journal, 788, 59
Williams J. P., Cieza L. A., 2011, ARA&A, 49, 67
Winter A. J., Clarke C. J., Rosotti G. P., 2019a, arXiv:1902.04586 [astro-ph]
Winter A. J., Kruijssen J. M. D., Chevance M., Keller B. W., Longmore S. N., 2019b, arXiv:1907.04602 [astro-ph]
van Terwisga S. E., Hacar A., van Dishoeck E. F., 2019, Astronomy and Astrophysics, 628, A85
van Terwisga S. E., et al., 2020, arXiv:2004.13551 [astro-ph]

This paper has been typeset from a TEX/LATEX file prepared by the author.